



Detailed chemistry modeling of rotating detonations with dilute *n*-heptane sprays and preheated air

Shan Jin^{a,b}, Chao Xu^c, Hongtao Zheng^a, Huangwei Zhang^{b,*}

^a College of Power and Energy Engineering, Harbin Engineering University, Harbin, 150001, China

^b Department of Mechanical Engineering, National University of Singapore, Singapore, 117576, Singapore

^c Energy Systems Division, Argonne National Laboratory, IL, 60439, United States

Received 5 January 2022; accepted 30 August 2022

Available online xxx

Abstract

Utilization of liquid fuels is crucial to enabling commercialization of rotating detonation engines (RDE) in the near future. In this study, Eulerian-Lagrangian simulations are conducted for rotating detonative combustion with dilute *n*-heptane sprays and preheated air. Two-dimensional flattened configuration is used and a skeletal chemical mechanism with 44 species and 112 elementary reactions for *n*-heptane combustion is adopted. The flow structure, droplet distribution, and thermochemical parameters in the refill zone are first analyzed. It is shown that the mixture in the refill zone is heterogeneous, including evaporating droplets, vapor, and air. When the total temperature is below 950 K, the average equivalence ratio increases with the total temperature. When it is higher than 950 K, the average equivalence ratio is almost constant. Subsequently, the chemical explosive mode analysis is applied to identify the controlling reactions and dominant combustion modes in the fuel refill zone and reaction fronts. Results demonstrate that the initiation reaction ($R104: n-C_7H_{16} + O_2 \rightarrow 2-C_7H_{15} + HO_2$) and low-temperature reaction ($R107: RO_2 \rightarrow R'O_2H$) are dominant in the upstream and downstream of the refill zone, respectively. The intermediate species from low-temperature chemistry, $R'O_2H$, is found to be important for the chemical explosive mode in the undetonated mixture. The influence of species diffusion and dispersed droplets is further analyzed. Results show that vapor autoignition facilitated by droplet evaporation occurs in the refill zone. Finally, the effects of the air total temperature on the detonation propagation speed and RDE propulsion performance are investigated. It is found that the detonation propagation speed and specific impulse increase with air total temperature. The total pressure ratio first increases and then decreases as the air total temperature increases. Moreover, when the total temperature of the preheated air is above 1,300 K, the effects of low-temperature chemistry are negligible.

© 2022 The Combustion Institute. Published by Elsevier Inc. All rights reserved.

Keywords: Rotating detonation; *N*-heptane sprays; Droplet evaporation; Total temperature; Low-temperature chemistry

* Corresponding author.

E-mail addresses: mpezhu@nus.edu.sg, huangwei.zhang@nus.edu.sg (H. Zhang).

<https://doi.org/10.1016/j.proci.2022.08.075>

1540-7489 © 2022 The Combustion Institute. Published by Elsevier Inc. All rights reserved.

1. Introduction

Rotating detonation engine (RDE) is deemed a promising pressure-gain combustion technology due to high thermodynamic cycle efficiency [1]. Fuel flexibility is crucial to materializing RDE towards a practical propulsion system. Typically, liquid fuels have high energy density and are convenient to be stored and transported. In recent years, the interests in liquid fuel RDE have revived. For instance, Bykovskii et al. successfully achieved two-phase rotating detonation waves (RDW) using kerosene sprays with oxygen-enriched air ($O_2/N_2 = 1:1$ by vol.) [2] or small addition of hydrogen or syngas [3]. They also found that hydrogen addition enables a more compact RDE combustor [3]. Kindracki [4] performed liquid kerosene with hydrogen addition in RDE experiments. Rotating detonations were successfully achieved, with a velocity deficit of 20%–25%, relative to Chapman-Jouguet (C-J) value. More recently, Wolański et al. [5] partially mixed preheated liquid Jet-A or gasoline with hot air, and the resultant reactant composition is higher than the rich flammability limit. They realized a rotating detonation without hydrogen addition. The RDW speed deficit is up to 35%, due to possible losses arising from chamber wall heat transfer, pre-injection deflagration, or reactant nonuniformity [5].

To shed further light on RDE with liquid fuels, numerical studies have also been available. For instance, Hayashi et al. [6] found that a steady JP-10/air RDW can be achieved within wide windows of equivalence ratio and pre-vaporization degree. They also reported that for certain JP-10 droplet concentration (e.g., 0.08–0.163 kg/m³ for 3 μ m droplets), detonation failure occurs. Moreover, Ren and Zheng [7] observed that under ramjet-like conditions rotating detonations with kerosene sprays (no pre-vaporization) can be achieved in a limited range of total pressure (5–7 atm) and increased total temperature is conducive to RDW stability. Besides, a bifurcated wave structure is observed near the spray injector [7].

Meng et al. [8] focused on a more volatile liquid fuel, *n*-heptane, and considered partially pre-vaporized *n*-C₇H₁₆ and air mixture to systematically evaluate the influences of droplet diameter (5–50 μ m) and pre-vaporization degree on detonation speed and evaporating fuel droplet distribution. They found that the detonation speed decreases with decreased pre-vaporization degree or increased droplet diameter. They also analyzed the detailed gas-liquid two-phase flow structure and found that a layer with high vapor concentration exists between the droplet-laden mixture/combustion product contact surface [9]. Besides, considering the same fuel, Zhao and Zhang [10] found that the detonation propagation speed

increases as the total equivalence ratio increases for the same droplet diameter. When the droplet diameter is less than 5 μ m, thrust force from kinetic energy and pressure gain decreases with droplet size. Beyond 5 μ m, the former first increases and then decreases with the droplet diameter, while the latter has limited change [10].

The key feature of liquid fuel RDE is that the combustion proceeds in vapor-droplet two-phase mixtures. Since preheated air is widely adopted in practical tests [5], this renders the static temperature and pressure of the undetonated mixture sufficiently high, probably inducing unexpected pre-RDW autoignition. It is shown that low-temperature chemistry (LTC) plays a significant role in autoignition process of liquid sprays in a hot atmosphere, featured by pronounced negative temperature coefficient (NTC) or zero temperature coefficient (ZTC) phenomenon [11]. However, due to the limitations of measurements and modeling approaches (simple chemistry, e.g., in [7][10]), under RDE conditions, how the oxidizer temperature affects the overall liquid fuel detonation performance, detailed chemical structure (particularly NTC effects), and fuel vapor distributions in the chamber are still not well understood. Meanwhile, the reaction progress in the fuel refill zone of a liquid fuel RDE with hot air has not been studied yet. To address the above questions, a fundamental study under RDE-relevant conditions is performed in this manuscript. We will conduct Eulerian–Lagrangian modeling of rotating detonations with dilute liquid *n*-heptane sprays. Different from our previous work [8–10], a detailed mechanism with 44 species and 112 elementary reactions [12] will be employed for *n*-heptane combustion. The objectives of our study are to clarify: (1) the thermochemical conditions in the heterogeneous fuel refill zone of a liquid fuel RDE; (2) the chemical structures in *n*-heptane rotating detonations; (3) the effects of preheated air total temperature and LTC on detonation speed and propulsion indices.

A two-dimensional (2D) configuration will be considered in this work. Here we are not aiming to model a real RDE burner based on the following reasons. Firstly, 2D model is sufficient to our research objectives; Secondly, nowadays it is still prohibitively expensive (maybe not affordable) to conduct direct numerical simulations of real RDE with realistic fuel (like *n*-heptane). If we model with LES and RANS, currently we are not certain if the existing the turbulence and turbulent combustion models, originally developed for low-speed flows, can be directly used for detonation modeling, due to considerable differences between deflagration and detonation. Meanwhile, detailed RDE experimental data (e.g., species or temperature in the chamber) suitable for model validations are very scarce. Therefore, before we move to reliable 3D modeling, we should first have progress in the

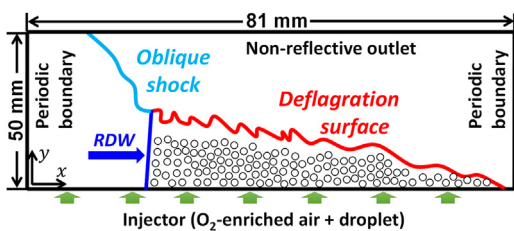


Fig. 1. Two-dimensional domain of a spray RDE.

above aspects, which still need many fundamental studies.

2. Physical model and numerical method

2.1. Physical model for spray RDE

Fig. 1 shows the 2D computational domain of a flattened model RDE chamber. Because the width of RDE is small compared to its length, the RDE domain can be “unrolled” into a 2D one due to the limited radial variation within the flow field. Past 2D simulations (e.g., Ref. [13] and [14]) suggest that the main RDC characteristics can be predicted reasonably well and the results achieved are insightful in understanding physics and performance relevant to practical RDE’s. The flow structure is composed of a RDW, deflagration surface, and oblique shock. The length (x -direction) and width (y) of the domain are 81 mm and 50 mm, respectively. Sensitivity analysis shows that doubling the domain length (see supplementary document) gives similar flow and reaction structures. As annotated in Fig. 1, the outlet is non-reflective, due to the local supersonic flows. Periodic conditions are enforced at the left and right sides, such that the RDW can propagate across the domain with continuous cycles.

The computational domain in Fig. 1 is discretized using $60 \times 60 \mu\text{m}^2$ Cartesian cells for the region of $[0, 25 \text{ mm}] \times [0, 81 \text{ mm}]$, whereas a cell size of $120 \mu\text{m}$ is used for the rest domain. The refined area can completely cover the RDWs in all simulations. This results in 648,000 cells for the domain in Fig. 1. Grid independence test with halved mesh size ($30 \mu\text{m}$, see supplementary document) shows that the flow and reaction structures are almost not changed.

Two-phase heterogeneous mixture is injected from a continuous inlet of the domain (at $y = 0$), including carrier gas and $n\text{-C}_7\text{H}_{16}$ droplets. The carrier gas is oxygen-enriched air ($Y_{\text{O}_2} : Y_{\text{N}_2} = 0.432 : 0.568$ by mass), which is deemed conducive for RDW stabilization by Bykovskii et al. [2]. Different from our previous studies [8–10], liquid fuel pre-vaporization prior to injection is not considered here and therefore $n\text{-C}_7\text{H}_{16}$ vapor mass fraction in the carrier gas is zero. The total pressure of the car-

rier gas is $p_0 = 20 \text{ atm}$ in all simulations. We run a series of spray RDE cases and find that when the total temperature, T_0 , is less than 700 K, the RDW cannot stabilize. A slightly higher critical temperature (1000 K) is reported in Ref. [7], which may be because less volatile fuel (i.e., kerosene) is considered in their simulations. In the following part of this paper, T_0 from 700 to 1400 K will be studied. The injections of $n\text{-C}_7\text{H}_{16}$ and air are determined by the isentropic relations between injector total pressure (p_0) and local pressure (p) near the inlet, and the droplet injection is synchronized with the carrier gas for both injection timing and velocity [9,10]. The details of injection condition can be found in Ref. [8]. Note that, when $p > p_0$, the inlet is treated as a solid wall and no backflow occurs.

The droplet initial temperature is assumed to be 323 K, to mimic pre-heating by the hot carrier gas in the upstream plenum, as implemented in the RDE tests by Kindracki [4] and Wolański et al. [5]. This enables efficient gasification of fuel droplets inside the combustion chamber and therefore promote detonative combustion efficiency. The initial material density and heat capacity of liquid n -heptane are 680 kg/m^3 and 2952 J/kg/K , respectively. Well sprayed (hence fine-grained) droplets are favorable for rotating detonations [4]. In this study, mono-sized droplets are considered, with the initial diameter $d_0 = 5 \mu\text{m}$. We only consider mono-disperse sprays in this study, because this is helpful to understand how a specific droplet size affects the detonation behaviors. Droplet aerodynamic breakup is modelled following Ref. [16]. The liquid fuel equivalence ratio ϕ is used to parameterize the droplet loading, defined as the mass ratio of the droplets to the oxidant. In our simulations, $\phi = 1$ is used for all cases.

2.2. Numerical method

The Eulerian–Lagrangian method is used to simulate rotating detonations with sprayed liquid fuel droplets. The gas phase is described with the Eulerian method, whilst the individual fuel droplets are tracked with a Lagrangian fashion. Two-way coupling between the gas and liquid phases are implemented, considering the exchanges of mass, momentum, and energy between them. For the gas phase, the Navier-Stokes equations of mass, momentum, total non-chemical energy, and species mass fraction are solved.

The point-force approximation is adopted for the liquid phase, and hence the droplet diameter should be smaller than the Eulerian cell size. Considering that the mesh size is $60 \mu\text{m}$, the droplets are essentially sub-grid. The effects of the dispersed droplets on the gas phase are considered through the source/sink terms, based on the Particle-source-in-cell (PSI-CELL) method [15]. The droplets are assumed to be spherical, and the temperature gradient inside the droplets is neglected, considering

their small Biot numbers (~ 0.057 when the droplet temperature and diameter are 323 K and $5 \mu\text{m}$). Droplet interactions (e.g., collisions) are not considered, which is not important for dilute sprays with initial droplet volume fraction less than 0.1%. Besides, the Basset force, lift force, and body force are not included. With these considerations, the evolutions of mass, momentum, and energy for a single droplet follow

$$\frac{dm_d}{dt} = -\dot{m}_d, \quad (1)$$

$$\frac{d\mathbf{u}_d}{dt} = \frac{\mathbf{F}_d + \mathbf{F}_p}{m_d}, \quad (2)$$

$$c_{p,d} \frac{dT_d}{dt} = \frac{\dot{Q}_c + \dot{Q}_{lat}}{m_d}, \quad (3)$$

where t is time and $m_d = \pi \rho_d d^3 / 6$ is the mass of a single droplet, with ρ_d and d being the droplet material density and diameter, respectively. \mathbf{u}_d is the droplet velocity vector, $c_{p,d}$ is the droplet heat capacity, and T_d is the droplet temperature.

The droplet evaporation rate \dot{m}_d in Eq. (1) is modelled as $\dot{m}_d = \pi d \rho_f D_f \tilde{Sh} \ln(1 + B_M)$ [17], where ρ_f and D_f respectively are the density and mass diffusivity at the film over the droplet surface. The Spalding mass transfer number is $B_M \equiv (Y_{Fs} - Y_{F\infty}) / (1 - Y_{Fs})$. Y_{Fs} and $Y_{F\infty}$ are the fuel vapor mass fractions at the droplet surface and in the gas phase, respectively. The modified Sherwood number \tilde{Sh} is $\tilde{Sh} = 2 + [(1 + Re_d Sc)^{1/3} \max(1, Re_d)^{0.077} - 1] / F(B_M)$, with the Schmidt number $Sc = 1.0$. The function $F(\vartheta) = (1 + \vartheta)^{0.7} \ln(1 + \vartheta) / \vartheta$ considers the variation of the film thickness due to Stefan flow effects [17]. In Eq. (2), the Stokes drag \mathbf{F}_d is modelled as $\mathbf{F}_d = (18\mu / \rho_d d^2) \cdot (C_d Re_d / 24) \cdot m_d (\mathbf{u} - \mathbf{u}_d)$ [18], where μ and \mathbf{u} are the gas dynamic viscosity and velocity vector, respectively. The drag coefficient, C_d , is estimated using Schiller and Naumann model [18]. $Re_d \equiv \rho d |\mathbf{u}_d - \mathbf{u}| / \mu$ is the droplet Reynolds number, and ρ is the gas density. Besides, $\mathbf{F}_p = -V_d \nabla p$ is the pressure gradient force and V_d is the droplet volume.

In Eq. (3), the convective heat transfer rate \dot{Q}_c is $\dot{Q}_c = h_c A_d (T - T_d)$. Here T is gas temperature, and A_d is the surface area of a single droplet. h_c is the convective heat transfer coefficient, following Ranz and Marshall [19]. Furthermore, \dot{Q}_{lat} accounts for the heat exchange rate associated with the latent heat of evaporation of liquid n -heptane.

The equations for the gas and liquid phases are solved using a customized OpenFOAM code, *RYrhoCentralFoam*. The solver is carefully validated and verified for shock capturing, molecular diffusion, flame-chemistry interactions and gas-liquid two-phase problems [20–22]. For gas phase, second-order backward scheme is used for time marching, and the time step is about

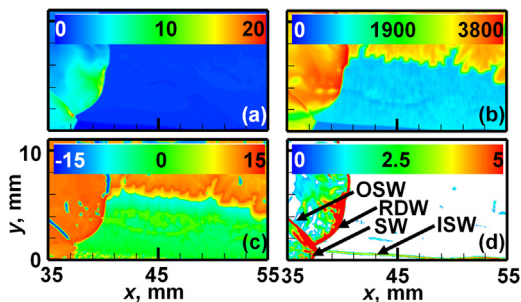


Fig. 2. Contours of (a) pressure (in MPa), (b) gas temperature (K), (c) logarithmic heat release rate, and (d) pressure gradient magnitude ($\times 10^9 \text{ Pa/m}$). $T_0 = 1000 \text{ K}$.

$2 \times 10^{-9} \text{ s}$. Second-order Godunov-type upwind-central scheme is employed to calculate the convection fluxes in the momentum equations. The total variation diminishing scheme is applied for the convection terms in energy and species equations. A detailed mechanism (44 species and 112 reactions) [12] is used. Low-temperature chemistry is included in this mechanism, and hence the LTC effects and two-stage ignition in n -heptane rotating detonations can be studied. One simulation with 88 species and 387 reactions (see details in supplementary document) is also run and the results demonstrate that differences between these two mechanisms are negligible.

For the liquid phase, fuel droplets are tracked from the barycentric coordinates. Equations (1) – (3) are integrated with first-order Euler method and the right-hand-side terms are treated in a semi-implicit approach. Details of the numerical method in *RYrhoCentralFoam* are available in [20–22].

The simulations are run on the ASPIRE 1 Cluster from National Supercomputing center in Singapore and 360 processors are used for each case. The simulated physical time is about 0.62 – 0.71 ms, corresponding to 10 cycles. To confirm that these cycles are sufficiently long, we also run cases with more than 10 cycles (see the supplementary document) and the results show that the detonation wave number is not changed and the average speeds are close.

3. Results and discussion

3.1. Thermochemical condition

Fig. 2 shows the distributions of pressure, gas temperature, heat release rate, and pressure gradient magnitude after the single-waved rotating detonation stabilizes (over ten cycles). For better illustration, the logarithmic heat release rate, LHRR, is plotted in Fig. 2(c), i.e., $\text{LHRR} \equiv \text{sign}[\text{HRR}] \cdot \log_{10}[1 + |\text{HRR}|]$.

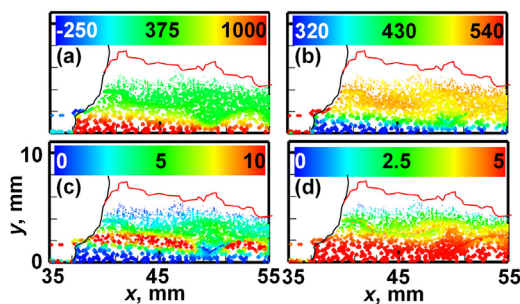


Fig. 3. Droplet (a) y -component velocity (in m/s), (b) temperature (K), (c) evaporation rate ($\times 10^{-9}$ kg/s), and (d) diameter (μm). $T_0 = 1000$ K. Black line: detonation/shock waves; red line: deflagration surface.

The carrier gas total temperature is $T_0 = 1000$ K. The basic structure of a RDE flow field is well captured. As seen from Fig. 2(b), the temperature in the fuel refill zone (enclosed by the RDW, deflagration surface, and inlet) varies between 510 and 950 K, and the mean is about 822 K. Besides, the pressure in the refill area is 1.78 atm – 11.5 atm with a mean of 10.68 atm. A notable feature in Fig. 2(c) is that although HRR is high along the RDW, detonative combustion does not maintain near the injector and only a shock wave can be found (marked as SW in Fig. 2d). A multi-wave structure can also be seen, connecting the induced shock wave (ISW), oblique shock wave (OSW) and the SW, as shown in Fig. 2(d). The ISW is induced by the high-speed injection of the air, which is also found in Ref. [23]. The gas between the ISW and the injector is featured by high speed, low temperature, and pressure. This therefore leads to slower propagation of the SW compared to the RDW. This also affects the heating, evaporation and movement of the liquid droplets in this area, which will be discussed in Fig. 3.

Plotted in Fig. 3 are the distributions of dispersed fuel droplets in the refill zone, and they are colored by their y -component velocity, temperature, evaporation rate, and diameter. After being injected into the combustor, the velocities of n -heptane droplets near the injector are relatively high before the ISW, up to 1000 m/s, and they gradually relax towards about 375 m/s. Meanwhile, as seen from Fig. 3(b), the droplets are quickly heated to their saturation temperature and start to vaporize. The droplet evaporation rate from Fig. 3(c) gradually increases (due to increased droplet temperature), peaks at 2 mm, and then decreases (due to decreased droplet mass) along the y -direction inside the refill zone.

Figs. 4(a) and 4(b) respectively show the distributions of the effective equivalence ratio, ϕ_{eff} , when the detonation wave propagates steadily at $T_0 = 700$ K and 1000 K. In this work, ϕ_{eff} is calculated from the ratio of required stoichiometric oxy-

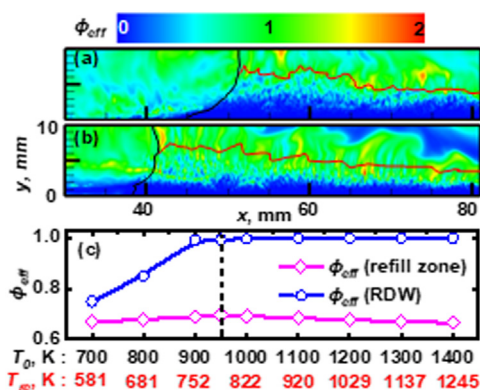


Fig. 4. Contours of effective equivalence ratio with $T_0 =$ (a) 700 K and (b) 1000 K. (c) Average effective equivalence ratio inside the fuel refill zone and at the detonation wave as functions of total temperature. Black line: detonation/shock waves; red line: deflagration surface. T_{re} : average static temperature in the refill zone.

gen atoms to the available oxygen atoms [24], i.e., $\phi_{eff} = 2(n_C + n_H/4)/n_O$, where n_C , n_H , and n_O denote the number of available carbon, hydrogen and oxygen atoms, respectively. Be reminded that since it is based on element conservation, ϕ_{eff} is also well defined in the product gas. However, the ones in the un-detonated mixtures (e.g., fuel refill zone) are irrelevant for our analysis. One can see from Fig. 4 that, very limited vapor (blue areas) exists near the injectors into the RDE chamber, and the starvation of fuel vapor leads to local detonation decoupling near the injector, as shown in Fig. 2(d).

As the air total temperature increases, more fuel vapor is present near the injector, through comparing Figs. 2(a) and 2(b). The variation of averaged effective equivalence ratio ϕ_{eff} under different T_0 is given in Fig. 4(c). The average static temperature T_{re} in the fuel refill zone at different T_0 is also given below the x -axis in Fig. 4(c). Here we average ϕ_{eff} respectively based on: (1) the refill zone (based on the criterion of local temperature lower than the corresponding T_0 , which is reasonable based on our examination of the 2D simulation results) and (2) detonation wave front ($\text{HRR} > 10^{13}$ J/m³/s [25]). We run one-dimensional simulations of gaseous detonations of n -heptane and oxygen-enriched air and find that utilizing this HRR to quantify detonation front is acceptable. In addition, we *a-posteriori* check the HRR at the detonation front from our 2D CFD results, and have the same conclusion. We also try to slightly vary the threshold (e.g., 5×10^{12} or 2×10^{13} J/m³/s), and in general our results are almost not affected. As T_0 increases from 700 K to 950 K, the average static temperature of the gas in the refill zone increases from 581 K to 787 K, the average ϕ_{eff} increases from 0.668 to 0.69. However, when T_0 further rises from 950 K to 1300 K, the average ϕ_{eff} in the refill zone is almost constant,

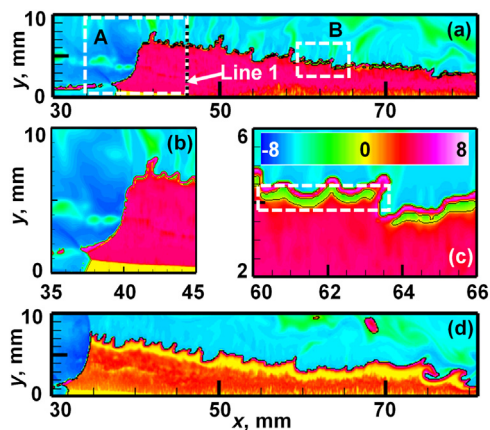


Fig. 5. Distributions of (a) CEM eigenvalue, close-up view of (b) zone A and (c) zone B, and (d) CEM eigenvalue without low-temperature chemistry for $T_0 = 1000$ K.

about 0.69, which is slightly higher than the lean flammability limit of *n*-heptane, 0.56 [26].

For the average ϕ_{eff} at the RDW, when $T_0 < 950$ K, a portion of liquid droplets cannot fully vaporize ahead of RDW, resulting in a relatively low ϕ_{eff} at the RDW in Fig. 4(c). As T_0 further increases, the remaining droplets after the RDW gradually decreases, and hence the equivalence ratio at the RDW is close to unity, which is the ER of the injected mixture in our simulations. Therefore, $T_0 = 950$ K is a critical total temperature for the ERs for the fuel vapor availability at the detonation wave. If we linearly extrapolate the three points of ϕ_{eff} (RDW) to 600 K, the corresponding ϕ_{eff} at the RDW is about 0.62, which is near the lean flammability limit. This also justifies why a stable RDW cannot be achieved with $T_0 < 700$ K under the simulated conditions.

3.2. Chemical structure

Here the chemical reaction characteristics in the spray RDE will be extracted with the chemical explosive mode analysis (CEMA) [27]. The equation for a gas reaction system reads:

$$\frac{D\omega(y)}{Dt} = \mathbf{J}_\omega \frac{Dy}{Dt} = \mathbf{J}_\omega(\omega + s + d), \quad \mathbf{J}_\omega = \frac{\partial \omega}{\partial y}, \quad (4)$$

where $D(\cdot)/Dt$ is the material derivative, y is the vector of temperature and species concentrations, ω is the chemical reaction, s is the diffusion term, d is the droplet evaporation term and \mathbf{J}_ω is the Jacobian of the chemical system. A chemical explosive mode (CEM) is defined as the eigen-mode associated with a positive (real part) eigenvalue which indicates that the local mixture tends to ignite under lossless conditions [27]. Distributions of the CEM eigenvalue λ_e are shown in Fig. 5

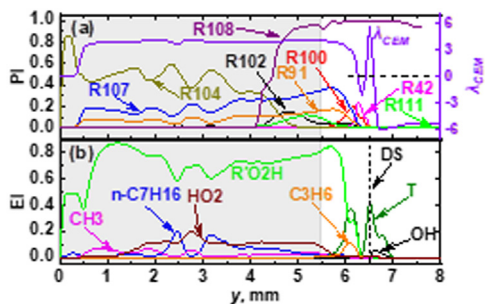


Fig. 6. Distributions of (a) PI and CEM logarithmic eigenvalue, and (b) EI at line #1 in Fig. 5. Shaded zone: droplet-laden area; DS: deflagration surface.

for $T_0 = 1000$ K. For better illustration, the logarithmic expression of the eigenvalue λ_e is plotted, i.e., $\lambda_{CEM} \equiv \text{sign}[\text{Re}(\lambda_e)] \cdot \log_{10}[1 + |\text{Re}(\lambda_e)|]$. Details of the CEMA can be found in [27].

Evident from Fig. 5(a) is that the heterogeneous two-phase mixture in the refill zone features large positive eigenvalues, indicating that fast droplet evaporation and vapor/air mixing turn the gas into chemically explosive state. Zero-crossing of the eigenvalue occurs at the detonation and deflagration surfaces. As shown in Fig. 5(b), ahead of the RDW, as the droplets are just sprayed into the chamber, the evaporation rate is low and the *n*-C₇H₁₆ vapor cannot mix effectively with the air, which results in overall fuel-lean composition (local ERs: 0–0.03) and the eigenvalue here is around zero. Near the deflagration surface shown in Fig. 5(c), some striped burned zones appear, with small negative eigenvalues (marked as dashed box). The reason for it will be further discussed in Fig. 6. For comparison, one additional simulation is run, in which the low-temperature elementary reactions, i.e., R105–R112 (see the reactions in Appendix A of [12]), are deactivated. Distribution of the CEM eigenvalue λ_{CEM} from this test is shown in Fig. 5(d). In the refill zone, λ_{CEM} is around 2, much lower than that of Fig. 5(a), i.e., about 4. This implies that the chemical timescale predicted with LTC included is approximately two orders of magnitude shorter than that without LTC. This clearly shows the LTC promotes the overall reactivity of the undetonated gaseous mixtures.

The chemical reactions in liquid *n*-heptane RDE will be further analyzed through the profiles of the participation index (PI) and explosion index (EI) [27] across the refill zone and the deflagration surface at $x = 45$ mm (annotated as line 1 in Fig. 5a). High PI (EI) signifies the dominance of the corresponding elementary reaction (species) in the explosive mode. The results are shown in Fig. 6. The curve of λ_{CEM} along line 1 is also plotted in Fig. 6(a). As seen from Fig. 6(a), the gas reactivity is weak (λ_{CEM} being very low, but still positive) near the injector, at $y < 0.5$ mm. This is

because very limited droplet evaporation and the low gas temperature (about 520 K) in the previously mentioned small region before the ISW. Beyond $y = 0.5$ mm, λ_{CEM} rises quickly and then levels around 4.0. Besides, at $y = 0-5.5$ mm (i.e., the shaded area, with heterogeneous mixtures of fuel droplets, vapor, and air), the initiation reaction R104 ($n\text{-C}_7\text{H}_{16} + \text{O}_2 \rightarrow 2\text{-C}_7\text{H}_{15} + \text{HO}_2$) is significant with the highest PI. After that, R107 ($\text{RO}_2 \rightarrow \text{R}'\text{O}_2\text{H}$), R111 ($\text{OR}''\text{O}_2\text{H} \rightarrow \text{OR}''\text{O} + \text{OH}$) and R91 ($1\text{-C}_7\text{H}_{15} \rightarrow 1\text{-C}_5\text{H}_{11} + \text{C}_2\text{H}_4$) become dominant. The first two reactions are low-temperature reactions and last one is a cracking reaction. For these locations, high EI of $\text{R}'\text{O}_2\text{H}$ is also observed, which is an intermediate species generated and consumed by the low-temperature reactions, R107 and R108 ($\text{R}'\text{O}_2\text{H} + \text{O}_2 \rightarrow \text{O}_2\text{R}'\text{O}_2\text{H}$), respectively.

Beyond the droplet-laden area (i.e., $y > 5.5$ mm), since the droplet evaporation is completed, the local mixture is gaseous (air and n -heptane vapor). The PIs for the LTC (e.g., R107) decrease. Instead, the PIs of the following elementary reactions become comparatively high: R42 ($\text{CH}_3 + \text{HO}_2 \rightarrow \text{CH}_3\text{O} + \text{OH}$), R100 ($n\text{-C}_7\text{H}_{16} + \text{OH} \rightarrow 2\text{-C}_7\text{H}_{15} + \text{H}_2\text{O}$) and R108 become dominant. At $y = 6.35$ mm, first zero-crossing of the λ_{CEM} curve can be found, corresponding to a high temperature EI (indicative of thermal runaway). Burned mixture next to it features $\lambda_{CEM} < 0$. This corresponds to the first-stage ignition (i.e., green areas in Fig. 5c), which produces small radicals such as C_3H_6 or C_2H_2 . Further downstream, the mixture becomes explosive again before it gets burned in the second-stage ignition near the reactant-product contact surface, with the λ_{CEM} being much higher than that before the first-stage ignition. This can also be corroborated from the EI of temperature in Fig. 6(b), and is consistent with the findings for n -heptane autoignition in Ref. [28]. Nonetheless, differently, our results indicate that thermal runaway are significant for both stages, which is because of sufficient radical runaway in both two-phase and gas-only mixtures in the refill zone.

The n -heptane vapor ignition modes in the refill zone are further analyzed in Fig. 7. Here the ignition mode is identified by projecting $D\omega(y)/Dt$ to the CEM using the left eigenvector \mathbf{b}_e [29]:

$$\frac{D\phi_\omega}{Dt} = \lambda_c\phi_\omega + \lambda_c\phi_s + \lambda_c\phi_d + \frac{D\mathbf{b}_e}{Dt} \cdot \boldsymbol{\omega}, \quad (5)$$

where $\phi_\omega = \mathbf{b}_e \cdot \boldsymbol{\omega}$, $\phi_s = \mathbf{b}_e \cdot \mathbf{s}$ and $\phi_d = \mathbf{b}_e \cdot \mathbf{e}$ respectively represent the projected chemical, diffusion and evaporation terms. Note that here ϕ_d include the thermal affect for the temperature. Note that the compressibility effect is not considered in this analysis, since it is insignificant in the refill zone, which is of interest here. The last term in Eq. (5) can be neglected, following Refs. [29]. The effects of species diffusion and droplet evaporation on gas reactions can be indicated respectively by the ratios of $\alpha_s = \phi_s/\phi_\omega$ and $\alpha_d = \phi_d/\phi_\omega$. If $\alpha > 1$,

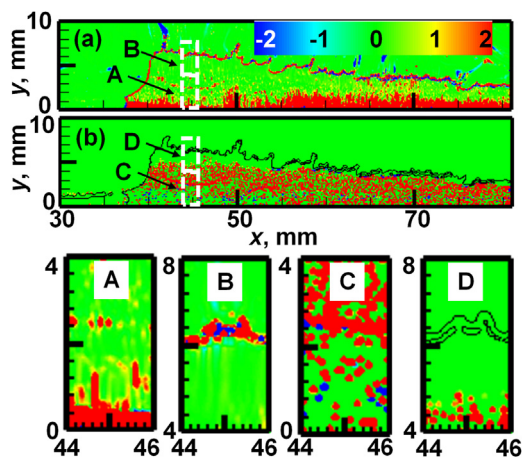


Fig. 7. Distributions (a) α_s , and (b) α_d and their enlarged views. $T_0=1000$ K. Black line in (b): isolines of $\lambda_{CEM} = 0$. A–D correspond to the boxes in Figs. (a) and (b).

ignition is facilitated by diffusion or droplet evaporation; if $|\alpha| < 1$, chemistry is dominant (hence autoignition); if $\alpha < -1$, diffusion or evaporation dominates chemistry and inhibits ignition [29].

The distributions of α_s and α_d in the refill zone are shown in Fig. 7. It can be seen from Fig. 7(a) that α_s is high (in red) near the spray injector in the entire refill zone, which can be clearly seen from the close-up view of zone A in Fig. 7(A). This indicates that the ignition of the local vapor is promoted by the species diffusion. This is understandable since in this region the equivalence ratio is still very low (see Fig. 4b), and efficient species diffusion (hence reactant mixing) is favorable for vapor ignition. Further downstream, e.g., $y > 5$ mm, the ignition mode changes to auto-ignition ($\alpha_s \approx 0$) and fuel diffusion plays a limited role. In these areas, the reactant composition is overall uniform, although reactant stratification still exists due to discrete distributions of the evaporating droplets. Near the deflagration surface (zone B), although diffusion is dominant, mixed local combustion modes are present in Fig. 7(B); the reactions at some pockets are inhibited by the species diffusion.

Likewise, how droplet evaporation affects vapor reaction ahead of the rotating detonation wave can be examined through the distributions of α_d . At the positions near the injector, the droplets are just sprayed into the chamber and cannot evaporate quickly, which results in small α_d , as shown in Figs. 7(b) and 7(C). As the droplet evaporation accelerates, its contribution towards the CEM becomes high (red spots in Fig. 7C) and is important for the entire droplet-laden refill zone. Nonetheless, some sparse blue dots are observed, which is probably due to the heat absorption by the evaporating droplets. Moving further downstream towards the deflagration front (Fig. 7D), the evaporation affect

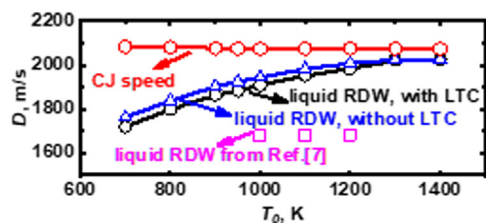


Fig. 8. Detonation wave speed versus total temperature.

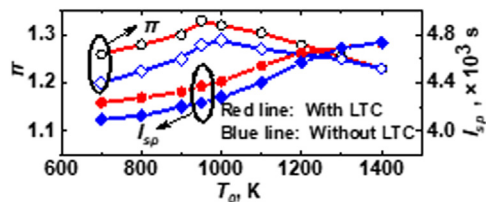


Fig. 9. Specific impulse and total pressure ratio versus total temperature.

becomes negligible as the droplets are fully evaporated.

3.3. Carrier gas total temperature effects

Fig. 8 shows the change of average detonation wave speed D with different air total temperatures T_0 . Here D is calculated from the pressure history at a probe near the head end of the domain. The Chapman–Jouguet speeds of gaseous n -heptane/air mixtures with $\phi = 1.0$ are added. The liquid fuel RDW speeds are 3%–15% lower than the C-J values. This may be caused by, e.g., imperfect reactant mixing and droplet evaporation [5][10]. It is also found that the RDW speed with liquid fuel increases when T_0 is increased, which is also observed by Meng et al. [9]. This is because the increase of T_0 raises the temperature in the fuel refill zone and increases the rate of mixing between reactants which and ultimately causes an increase in D . This trend is different from the result of Ref. [7], because the droplets in [7] are finer ($2 \mu\text{m}$), which enables complete evaporation before the RDW arrives and therefore the equivalence ratio of the undetonated gas has weak dependence on T_0 . In addition, the average speeds predicted without LTC are higher than those with LTC. This is because the low-temperature chemical reactions in the fuel refill zone consumes part of the gaseous $n\text{-C}_7\text{H}_{16}$.

Fig. 9 shows the effects of air total temperature on the total pressure ratio π and specific impulse I_{sp} . The pressure ratio is $\pi = p_3/p_0$, where p_3 is the total pressure near the exit ($y = 49 \text{ mm}$) and p_0 is air injection total pressure, i.e., 20 atm in this study. The specific impulse is calculated following Ref. [10]. One can see that the pressure ratio first increases and then decreases with increasing T_0 . From $T_0 = 700 \text{ K}$ to 950 K , an increase in T_0

changes the effective equivalence ratio at the RDW (see Fig. 4), which causes a gradual increase in p_3 and ultimately an increase in π . From 1000 K to 1400 K , the average equivalence ratio at the RDW front no longer changes with increasing T_0 . However, as T_0 increases, chemical reactions accelerate, the deflagrative combustion intensifies and thus lowers the detonated fuel fraction and p_3 , which eventually leads to a decrease in the pressure ratio (the detonated fuel fraction versus total temperature is shown in supplementary document for interested readers).

Nonetheless, the specific impulse monotonically increases with T_0 . This is because injection with higher air total temperature expands the area of the low-temperature region before the ISW mentioned in Section 3.1. The gas velocity in the mentioned region is high (more than 1000 m/s). The increase of the area increases the gas velocity and eventually increases the specific impulse.

The results predicted without LTC are also shown. One can find that the I_{sp} without LTC is consistently underpredicted. This is because the deactivation of the LTC changes CEM eigenvalue λ_e (lower reactivity, see Fig. 5) in the refill zone. The change in the CEM eigenvalue results in a lower detonated fuel fraction in the detonation combustion (see supplementary document), thereby a lower pressure of the detonation wave and ultimately to a lower specific impulse and pressure ratio. When $T_0 > 1300 \text{ K}$, the propulsion indices are almost not affected by the LTC, because the LTC is inhibited for this temperature range.

4. Conclusion

Two-dimensional rotating detonations with liquid n -heptane sprays and preheated air are simulated with a Eulerian-Lagrangian method and a skeletal chemical mechanism. The results show that the mixture in the refill zone is heterogeneous, including evaporating droplets, vapor, and air. When the total temperature is below 950 K , the average equivalence ratio increases with the total temperature. The chemical structures in the refill zone and reaction front are studied with the chemical explosive mode analysis. It is seen that with fuel vapor addition and efficient mixing, the mixture becomes explosive in most of the refill zone. The initiation reaction (R104) and low-temperature reaction (R107) are dominant in the upstream and downstream of the refill zone, respectively. The LTC intermediate species, $\text{R}'\text{O}_2\text{H}$, is found to be important for chemical explosive mode in the undetonated mixture. The influence of species diffusion and dispersed droplets on fuel vapor ignition is further analyzed. The detonation propagation speed and specific impulse increase with air total temperature. The total pressure ratio firstly increases and then slightly decreases. Inclusion of the LTC in the

chemical mechanism would affect the predictions of these parameters, but the difference is minimized when the air total temperature is above 1300 K.

Declaration of Competing Interest

none.

Acknowledgements

Shan Jin is supported by the CSC Scholarship. This work used the computational resources of The ASPIRE 1 Cluster in National Supercomputing center, Singapore.

Supplementary materials

Supplementary material associated with this article can be found, in the online version, at doi:10.1016/j.proci.2022.08.075.

References

- [1] V. Anand, E. Gutmark, Rotating detonation combustors and their similarities to rocket instabilities, *Prog. Energy Combust. Sci.* 73 (2019) 182–234.
- [2] F.A. Bykovskii, S.A. Zhdan, E.F. Vedernikov, Continuous spin detonation of fuel-air mixtures, *Combust. Explos. Shock Waves* 42 (2006) 463–471.
- [3] F.A. Bykovskii, S.A. Zhdan, E.F. Vedernikov, Continuous detonation of the liquid kerosene—air mixture with addition of hydrogen or syngas, *Combust. Explos. Shock Waves* 55 (2019) 589–598.
- [4] J. Kindracki, Experimental research on rotating detonation in liquid fuel–gaseous air mixtures, *Aerosp. Sci. Technol.* 43 (2015) 445–453.
- [5] P. Wolański, W. Balicki, W. Perkowski, A. Bilar, Experimental research of liquid-fueled continuously rotating detonation chamber, *Shock Waves* (2021) 1–6.
- [6] A.K. Hayashi, N. Tsuboi, E. Dzieminska, Numerical study on JP-10/air detonation and rotating detonation engine, *AIAA J* 58 (2020) 5078–5094.
- [7] Z. Ren, L. Zheng, Numerical study on rotating detonation stability in two-phase kerosene-air mixture, *Combust. Flame* 231 (2021) 111484.
- [8] Q. Meng, M. Zhao, H. Zheng, H. Zhang, Eulerian-Lagrangian modelling of rotating detonative combustion in partially pre-vaporized n-heptane sprays with hydrogen addition, *Fuel* 290 (2021) 119808.
- [9] Q. Meng, N. Zhao, H. Zhang, On the distributions of fuel droplets and in situ vapor in rotating detonation combustion with pre-vaporized n-heptane sprays, *Phys. Fluids* 33 (2021) 43307.
- [10] M. Zhao, H. Zhang, Rotating detonative combustion in partially pre-vaporized dilute n-heptane sprays: droplet size and equivalence ratio effects, *Fuel* 304 (2021) 121481.
- [11] Z. Bouali, C. Pera, J. Reveillon, Numerical analysis of the influence of two-phase flow mass and heat transfer on n-heptane autoignition, *Combust. Flame* 159 (2012) 2056–2068.
- [12] S. Liu, J.C. Hewson, J.H. Chen, H. Pitsch, Effects of strain rate on high-pressure nonpremixed n-heptane autoignition in counterflow, *Combust. Flame* 137 (2004) 320–339.
- [13] J. Fujii, Y. Kumazawa, A. Matsuo, S. Nakagami, K. Matsuoka, J. Kasahara, Numerical investigation on detonation velocity in rotating detonation engine chamber, in: *Proc. Combust. Inst.*, 2016.
- [14] D. Schwer, K. Kailasanath, Numerical investigation of the physics of rotating-detonation-engines, in: *Proc. Combust. Inst.* 33, 2011, pp. 2195–2202.
- [15] C.T. Crowe, M.P. Sharma, D.E. Stock, The particle-source-in cell (PSI-CELL) model for gas-droplet flows 99 (1977) 325–332.
- [16] A. Omidvar, Development and assessment of an improved droplet breakup model for numerical simulation of spray in a turbulent flow field, *Appl. Therm. Eng.* 156 (2019) 432–443.
- [17] B. Abramzon, W.A. Sirignano, Droplet vaporization model for spray combustion calculations, *Int. J. Heat Mass Transf.* 32 (1989) 1605–1618.
- [18] A.B. Liu, D. Mather, R.D. Reitz, Modeling the effects of drop drag and breakup on fuel sprays, *SAE Trans* (1993) 83–95.
- [19] W.E. Ranz, J.W.R. Marshall, Evaporation from Drops, Part I, *Chem. Eng. Prog.* 48 (1952) 141–146.
- [20] M. Zhao, Z.X. Chen, H. Zhang, N. Swaminathan, Large eddy simulation of a supersonic lifted hydrogen flame with perfectly stirred reactor model, *Combust. Flame* 230 (2021) 111441.
- [21] Z. Huang, M.J. Cleary, Z. Ren, H. Zhang, Large eddy simulation of a supersonic lifted hydrogen flame with sparse-Lagrangian multiple mapping conditioning approach, *Combust. Flame* 230 (2021) 119402.
- [22] Z. Huang, M. Zhao, Y. Xu, G. Li, H. Zhang, Eulerian-Lagrangian modelling of detonative combustion in two-phase gas-droplet mixtures with OpenFOAM: validations and verifications, *Fuel* 286 (2021) 119402.
- [23] R. Zhou, J.-P. Wang, Numerical investigation of flow particle paths and thermodynamic performance of continuously rotating detonation engines, *Combust. Flame* 159 (2012) 3632–3645.
- [24] R. Zhou, S. Hochgreb, The behaviour of laminar stratified methane/air flames in counterflow, *Combust. Flame* 160 (2013) 1070–1082.
- [25] M. Zhao, M.J. Cleary, H. Zhang, Combustion mode and wave multiplicity in rotating detonative combustion with separate reactant injection, *Combust. Flame* 225 (2021) 291–304.
- [26] I. Glassman, R.A. Yetter, N.G. Glumac, in: *Combustion*, Academic press, Waltham USA, 2014, p. 708.
- [27] T.F. Lu, C.S. Yoo, J.H. Chen, C.K. Law, Three-dimensional direct numerical simulation of a turbulent lifted hydrogen jet flame in heated coflow: a chemical explosive mode analysis, *J. Fluid Mech.* 652 (2010) 45–64.
- [28] R. Shan, C.S. Yoo, J.H. Chen, T. Lu, Computational diagnostics for n-heptane flames with chemical explosive mode analysis, *Combust. Flame* 159 (2012) 3119–3127.
- [29] C. Xu, J.-W. Park, C.S. Yoo, J.H. Chen, T. Lu, Identification of premixed flame propagation modes using chemical explosive mode analysis, in: *Proc. Combust. Inst.* 37, 2019, pp. 2407–2415.